

Eco-friendly Synthesis of TiO₂ Nanoparticles from *Azadirachta indica* and *Psidium guajava* Leaves for Antibacterial and Dye Degradation Applications

R. Leethiyal¹, S. Gopi², M. Vadivel³

^{1,2,3}Department of Physics, Sri Ramakrishna Mission Vidyalaya College of Arts and Science Coimbatore, India.

¹Department of Physics, Nirmala College for Women, Coimbatore, India.

Abstract

This research explores an eco-friendly approach to synthesizing titanium dioxide (TiO₂) nanoparticles using aqueous leaf extracts from *Azadirachta indica* (neem) and *Psidium guajava* (guava). This method presents a green alternative to conventional chemical synthesis. The biosynthesized nanoparticles were characterized using XRD, FTIR, UV-Vis, PL, FESEM, and EDAX techniques. The XRD analysis confirmed the crystalline structure of the synthesized nanoparticles, while FTIR analysis revealed the presence of active biomolecules involved in the reduction and stabilization of the nanoparticles. UV-Vis and PL analyses revealed the optical properties, and FESEM images showed well-defined spherical structures. EDAX confirmed the elemental purity with minimal impurities. The nanoparticles exhibited excellent photocatalytic degradation of methylene blue under UV irradiation and demonstrated potent antibacterial activity against *Staphylococcus aureus* and *Escherichia coli*. The outcomes emphasize the potential of these green-synthesized TiO₂ NPs in wastewater treatment and antimicrobial applications.

Keywords: TiO₂ nanoparticles, Green synthesis, *Psidium guajava*, *Azadirachta indica*, Antibacterial activity, Photocatalytic degradation

1. Introduction

Titanium dioxide (TiO₂) nanoparticles have gained significant attention as a versatile material in the field of nanotechnology, showing promising results in environmental remediation, biomedical applications, and catalysis [20]. Conventional physical and chemical methods of synthesizing TiO₂ nanoparticles often employ hazardous chemicals and require significant energy input. As a sustainable alternative, green synthesis methods utilizing plant extracts have gained attention for being cost-effective, safe, and environmentally benign [17, 21]. Plant extracts contain bioactive phytochemicals - such as flavonoids, alkaloids, terpenoids, and polyphenols - that function as reducing, stabilizing, and capping agents during nanoparticle formation. Several studies have been reported the use of different plant species like *Annona squamosa*, *Catharanthus roseus*, and *Psidium guajava* in the green synthesis of TiO₂ [5]. In particular, *Azadirachta indica* (neem) and *Psidium guajava* (guava) are well-known for their rich phytochemical content and medicinal value, making them ideal candidates for nanoparticle biosynthesis [1]. The

enhanced surface area, high reactivity, and stability of TiO₂ NPs compared to their bulk counterparts make them suitable for various applications. One critical area of application is photocatalysis, especially for the degradation of industrial dyes and pharmaceutical contaminants such as tetracycline (TC) [3]. However, the performance of TiO₂ in photocatalysis is limited due to its large band gap (3.2 eV) and high recombination rate of charge carriers [4]. The environmental impact of synthetic dyes and antibiotics in aquatic systems is a growing concern, and conventional water treatment methods often prove inadequate. The use of nanomaterials like TiO₂ has shown high potential in addressing these issues [7].

In this study, TiO₂ nanoparticles synthesized using neem and guava leaf extracts were evaluated for their antibacterial and photocatalytic capabilities. The findings highlight the potential for these plant-based nanomaterials in sustainable water purification technologies.

2. Materials and Methods

2.1 Materials

Titanium(IV) isopropoxide (TTIP, 97%, Sigma-Aldrich) served as the precursor material. Methylene blue dye (97%, Nice Chemicals) was used for photocatalytic degradation experiments. Distilled water was used throughout.

2.2 Collection and Preparation of Leaf Extracts

Fresh leaves of *A. indica* (Neem) and *P. guajava* (Guava) were collected from Rathinapuri, Coimbatore. After thorough washing with tap water and rinsing with deionized water to remove dirt and soil particles [8], the leaves were chopped into small pieces. For extraction, 80 mL of distilled water was heated with the leaves at 80°C for 30 minutes [15]. The extracts were then filtered and stored for further use.

2.3 Green Synthesis of TiO₂ Nanoparticles

The synthesis was performed using a co-precipitation technique. TTIP (5 mL) was dissolved in 8 mL of distilled water and stirred at 40°C for 30 minutes. Filtered guava and neem leaf extracts (50 mL) were added dropwise to this solution under constant stirring. The resulting precipitate was filtered, dried, and annealed at 600°C for 3 hours to obtain crystalline TiO₂ nanoparticles.

3. Applications

3.1 Antibacterial Activity

The antibacterial activity of the biosynthesized TiO₂ nanoparticles was assessed using the agar well diffusion method against *Staphylococcus aureus* and *Escherichia coli*. Wells were loaded with varying concentrations of the TiO₂ nanoparticle solution (25 µL, 50 µL, 75 µL, and 100 µL). The inoculated plates were then incubated at 37°C for 24 hours, after which the zones of inhibition were measured to evaluate antibacterial efficacy.

3.2 Photocatalytic Activity

Photocatalytic degradation of methylene blue was carried out under UV light. A 50 mL solution of MB dye was mixed with 5 mg of biosynthesized TiO₂ NPs and left in the dark for 30 minutes to attain adsorption equilibrium. The mixture was then irradiated using two 20W UV lamps, and samples were withdrawn at intervals of 5 minutes up to 30 minutes. Degradation efficiency was determined using a UV-Vis spectrophotometer (JASCO V-760).

4. Characterization Techniques

- XRD (PANalytical X'Pert Pro) confirmed crystalline phases.

- FTIR (JASCO FT/IR-4700 Type A) identified key functional groups from plant extracts.
- UV-Vis spectroscopy (JASCO V-770) evaluated absorbance properties.
- PL spectroscopy was used to assess the recombination behaviour of charge carriers.
- FESEM (TESCAN MIRA3) provided insight into nanoparticle morphology.
- EDAX analysis confirmed elemental composition with minimal contamination.

4. Results and discussion

4.1 XRD Analysis

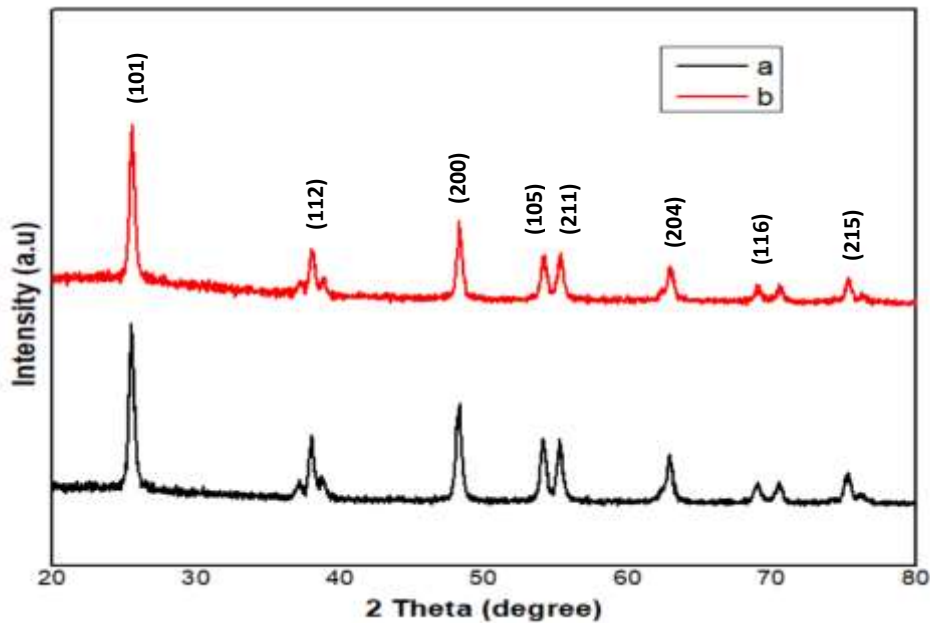


Figure. 1 XRD pattern of Biosynthesized TiO₂

(a) *A. indica* (Neem) & (b) *P. guajava* (Guava)

X-ray diffractogram of biosynthesized materials calcined at 600 °C has been presented in Figure 1. The biosynthesized TiO₂ nanoparticles displayed distinct diffraction peaks that are in good agreement with the standard tetragonal anatase phase, as referenced by JCPDS card No. 21-1272. The anatase peaks are found at 2θ values of 25.54°, 38.04°, 48.25°, 54.20°, 62.91°, 69.04°, and 75.42°, corresponding to the (101), (112), (200), (105), (211), (204), (116) and (215) crystal planes [8].

The average crystallite size of the nanoparticles can be estimated using Debye Scherrer formula

$$D = \frac{0.9\lambda}{\beta \cos\theta} \text{ (nm)}$$

where, D - crystallite size in nm, λ - the wavelength in nm, β - full width half maximum value in radian and θ - diffraction angle in degree.

Also, the lattice constants of TiO₂ nanoparticles were calculated using the following equation [11].

$$\frac{1}{d^2} = \frac{h^2 + k^2}{a^2} + \frac{l^2}{c^2}$$

Where, d is the interplanar distance and h, k and l are the miller indices. Moreover, a and c are lattice parameters of tetragonal structure.

The calculated crystallite size and lattice parameters of prepared TiO₂ nanoparticles were shown in the Table 1.1.

Table 1.1 Lattice parameter and average grain size of prepared Biosynthesized TiO₂ NPs

S. No	Biosynthesized TiO ₂ Sample	Lattice Constant (Å)			Crystallite Size (nm)
		a	c	c/a ratio	
1.	<i>A. indica</i> (Neem)	3.77	9.1	2.41	22.7
2.	<i>P. guajava</i> (Guava)	3.77	8.77	2.33	17.2

Standard JCPDS Card no. (89-4921) a = 3.777 (Å) c = 9.501 (Å) [8].

The decrease in lattice parameters and crystallite size, along with a lower c/a ratio observed in TiO₂ nanoparticles synthesized using Neem and Guava leaf extracts, suggests effective incorporation of phytochemicals from the leaf extracts into the TiO₂ crystal lattice [8]. The Guava leaf extract, in particular, contains bioactive molecules that function as both capping and reducing agents during the synthesis process. These phytochemicals interact with the growing TiO₂ nuclei and preferentially inhibit expansion along the c-axis, leading to a reduced c/a ratio and a slightly smaller crystallite size when compared to the sample synthesized using Neem extract

4.2 FTIR Analysis

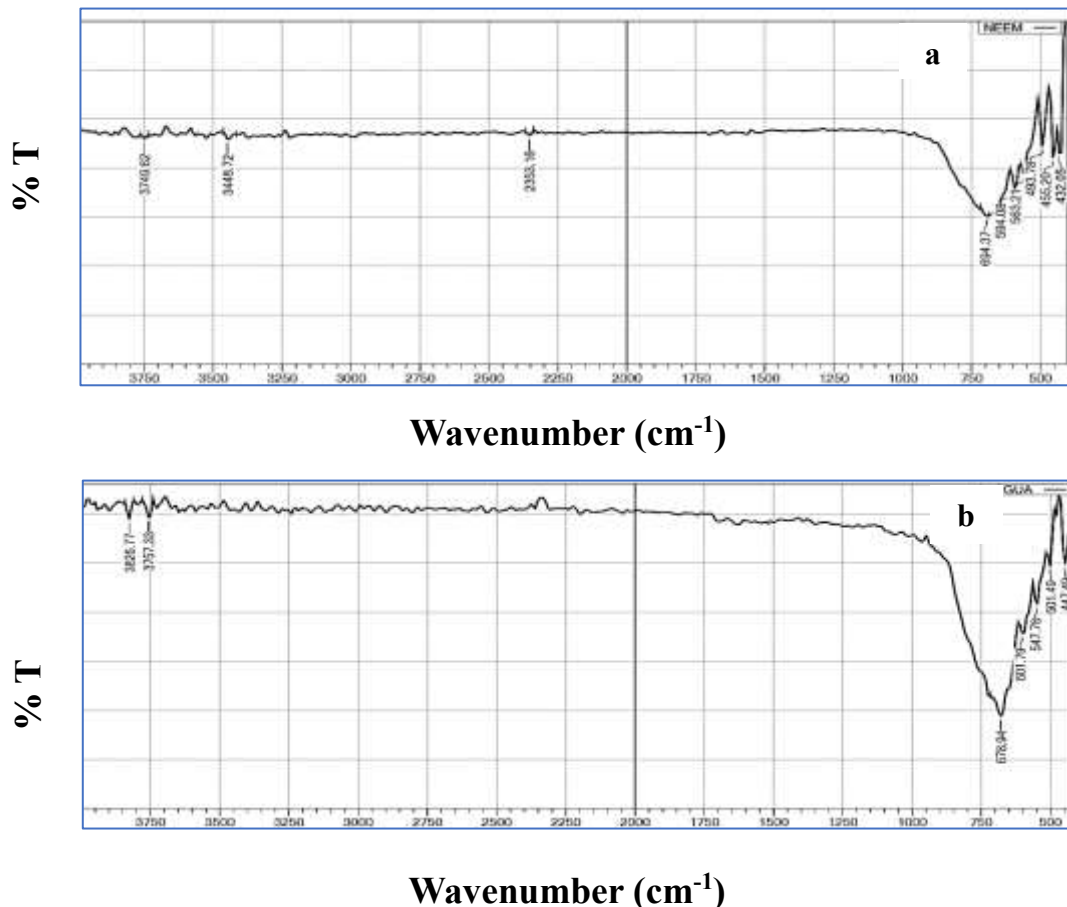
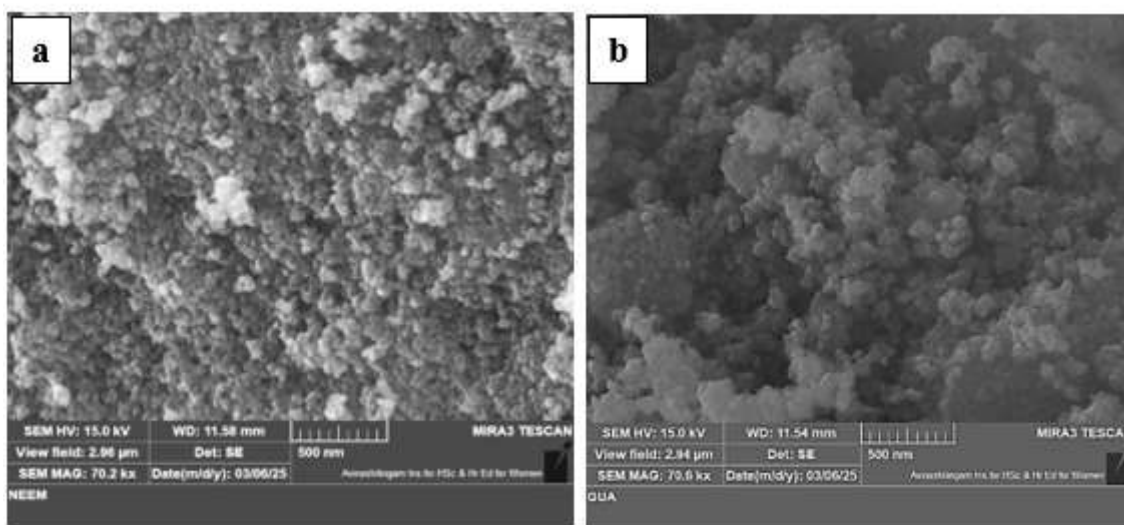


Figure. 2 FTIR spectra of Biosynthesized TiO₂ nanoparticles

(b) *A. indica* (Neem) & (b) *P. guajava* (Guava)

The FTIR spectra of TiO₂ nanoparticles synthesized using *Azadirachta indica* (neem) and *Psidium guajava* (guava) leaf extracts, as indicated in Figure 2, reveal the presence of functional groups that confirm the involvement of plant-derived phytochemicals in the green synthesis process. In the neem-mediated synthesis, broad bands at 3749.62 cm⁻¹ and 3448.72 cm⁻¹ correspond to O–H stretching vibrations from hydroxyl groups, indicating the presence of phenols or alcohols [2], while a peak at 2353.16 cm⁻¹ is attributed to C=O stretching, possibly from carbon dioxide or carboxylic acids. Strong absorptions between 694.33 cm⁻¹ and 432.05 cm⁻¹, along with additional bands at 594.08, 659.26, 843.78, and 913.87 cm⁻¹, indicate Ti–O–Ti and Ti–O stretching vibrations, confirming the formation of TiO₂ and suggesting the presence of anatase or rutile phases [14]. Similar observations were also reported by B.K. Thakur et al. (2019) [2]. Similarly, the FTIR spectrum of guava-mediated TiO₂ nanoparticles shows broad O–H stretching peaks at 3862.77 cm⁻¹ and 3757.33 cm⁻¹, along with strong absorption bands in the 678.94–447.49 cm⁻¹ range, confirming Ti–O bond formation. Additional peaks at 601.79, 547.78, and 501.49 cm⁻¹ further support the presence of metal–oxygen bonds. The absence of strong signals in the mid-infrared range (1500–2500 cm⁻¹) in the guava spectrum suggests fewer interfering organic residues, indicating a cleaner synthesis. Overall, both spectra confirm the key role of bioactive compounds like flavonoids, terpenoids, and polyphenols in reducing titanium precursors and stabilizing the nanoparticles [2], validating the green synthesis of TiO₂ using neem and guava leaf extracts.

4.3 Morphology and Compositional Analysis



**Figure. 3 FESEM images of Biosynthesized TiO₂ nanoparticles
(a) *A. indica* (Neem) & (b) *P. guajava* (Guava)**

In Figure 3, the Field Emission Scanning Electron Microscopy (FESEM) images of TiO₂ nanoparticles synthesized using *Azadirachta indica* (neem) and *Psidium guajava* (guava) leaf extracts exhibit a consistent nanoscale morphology characterized by densely packed, roughly spherical, and agglomerated particles with sizes predominantly below 100 nm. In the neem-mediated synthesis, the nanoparticles exhibit a uniform distribution and smooth contours, suggesting a semi-crystalline or amorphous nature, with clustering attributed to the bio-organic compounds in neem extract acting as natural reducing and stabilizing agents. Similarly, the guava-mediated synthesis displays a highly aggregated surface morphology with spherical nanoparticles and a rough surface texture, likely due to residual

phytochemicals from the guava extract serving as capping and stabilizing agents [12, 13]. Both extracts promote particle stability and prevent uncontrolled growth, although slight agglomeration is observed, which is typical in green synthesis due to intermolecular interactions such as hydrogen bonding and van der Waals forces. The absence of irregular particles or foreign contaminants in both cases indicates high purity and successful nanoparticle formation. These morphological characteristics confirm the efficiency of neem and guava leaf extracts in the biosynthesis of TiO₂ nanoparticles and highlight their potential applicability in photocatalytic, antibacterial, and environmental remediation applications.

4.4 EDX Analysis

The elemental composition of TiO₂ nanoparticles synthesized using *Azadirachta indica* (neem) and *Psidium guajava* (guava) leaf extracts was confirmed through Energy Dispersive X-ray (EDX/EDAX) analysis shown in the figure 4. The spectra revealed prominent peaks corresponding to titanium (Ti) and oxygen (O), the major constituents of TiO₂, confirming the successful formation of titanium dioxide nanoparticles in both cases [16]. For neem-synthesized TiO₂, titanium showed a high weight percentage (52.64%) and net intensity (433.48), while oxygen was present at 37.13% by weight and 54.33% by atomic percentage. Carbon was also observed in a more significant amount (10.23% by weight, 19.94% by atomic percentage), attributed to the organic constituents of the neem extract, which function as effective capping and stabilizing agents. The Ti peak was prominently located around 4.5–5 keV, and the O peak near 0.5 keV, which are characteristic signatures of TiO₂. The relatively low error percentages for Ti (2.29% in guava, 2.46% in neem) indicate reliable detection, while slightly higher errors for O and C are acceptable due to their lower atomic masses and possible spectral overlaps. Similarly, for guava-synthesized TiO₂, titanium exhibited the highest weight percentage (65.24%) and a substantial atomic percentage (38.25%), while oxygen showed a weight percentage of 33.50% and an atomic percentage of 58.81%, consistent with the expected stoichiometry of TiO₂. A minor carbon peak (1.26% by weight, 2.94% by atomic percentage) was also detected, likely originating from the phytochemicals in guava leaves that act as natural reducing and stabilizing agents during the green synthesis process. The absence of peaks related to other metallic impurities in both samples further supports the high purity of the synthesized nanoparticles. Overall, the EDAX analysis validates the elemental composition and purity of the green-synthesized TiO₂ nanoparticles and highlights the efficiency of both neem and guava leaf extracts as effective biogenic agents for nanoparticle formation, offering a sustainable and eco-friendly approach to nanomaterial synthesis.

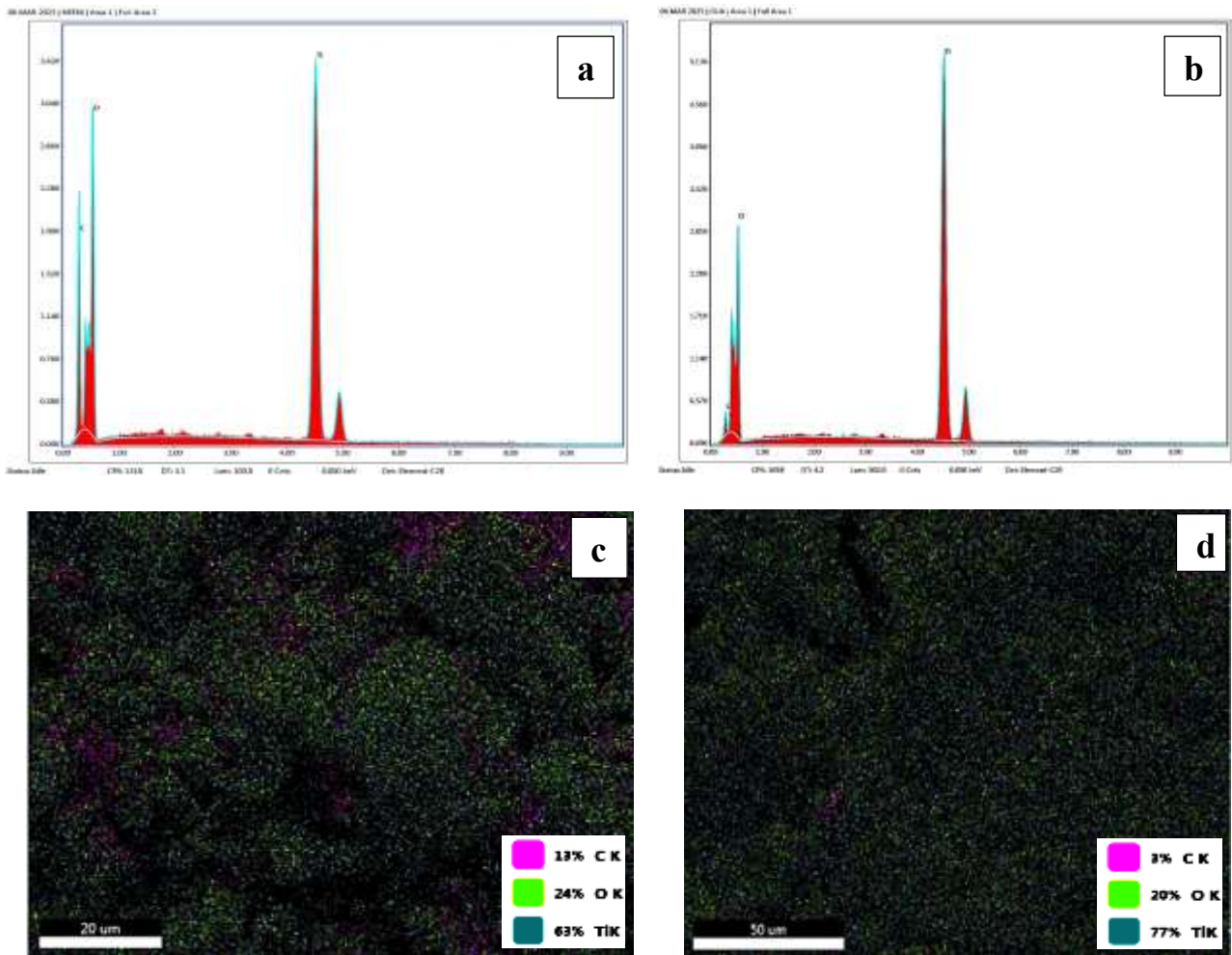


Figure. 4 EDX spectra of Biosynthesized TiO₂ nanoparticles (a,c) *A. indica* (Neem) & (b,d) *P. guajava* (Guava)

4.5 Optical Absorption Studies

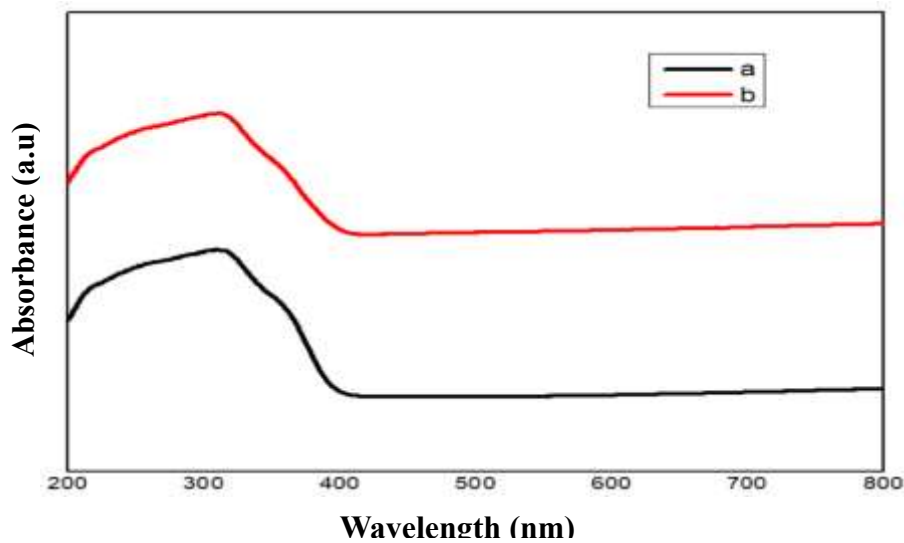


Figure. 5 UV-Vis absorption spectra of Biosynthesized TiO₂ nanoparticles (a) *A. indica* (Neem) & (b) *P. guajava* (Guava)

The UV-Vis absorption spectra of TiO₂ nanoparticles synthesized using *Azadirachta indica* (Neem) and *Psidium guajava* (Guava) leaf extracts, as shown in Figure 5, display characteristic optical behavior within the 200–800 nm wavelength range. The TiO₂ nanoparticles derived from Neem exhibit an absorption peak at 313 nm, while those from Guava show a peak at 314 nm. These absorption edges correspond to the fundamental electronic transitions in the material. The bandgap energy (E_g) of the TiO₂ nanoparticles from *A. indica* (Neem) and *P. guajava* (Guava) was calculated using the following equation [8].

$$E_g = \frac{hc}{\lambda} \text{ (eV)}$$

where h is the Planck's constant, c is the velocity of light and λ is the wavelength (absorption edge). The band gap energy of *A. indica* (Neem) and *P. guajava* (Guava) TiO₂ nanoparticles were 4.04 eV and 4.03 eV respectively.

4.6. Photoluminescence studies

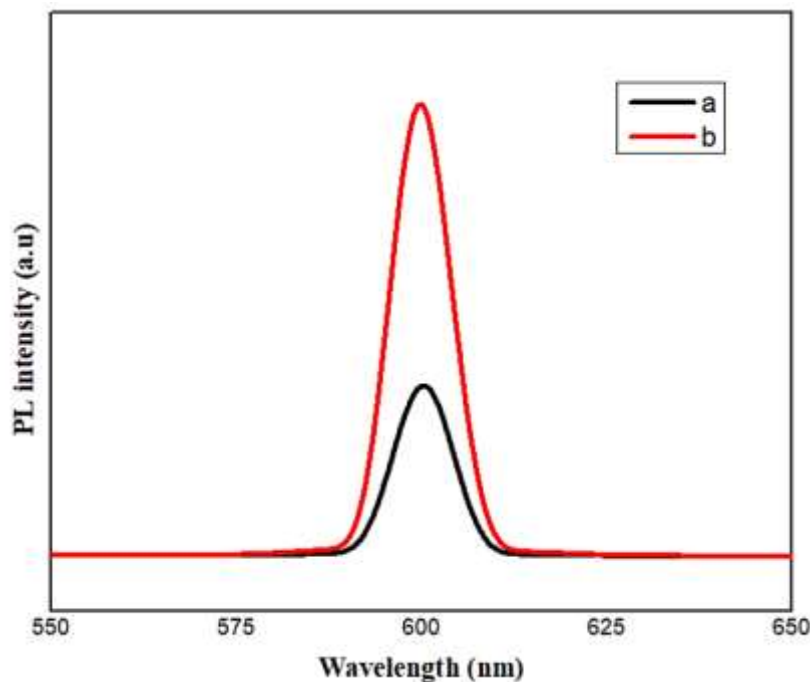


Figure. 6 PL spectra of Biosynthesized TiO₂ nanoparticles (a) *A. indica* (Neem) & (b) *P. guajava* (Guava)

The optical and photoelectronic properties of the prepared nanoparticles were investigated using the photoluminescence (PL) spectrum. The main cause of photoluminescence emission in semiconductors is primarily due to the radiative recombination of electrons and holes in the semiconductor materials [8]. Figure 6 shows the PL spectra of biosynthesized TiO₂ nanoparticles derived from *Azadirachta indica* (Neem) and *Psidium guajava* (Guava), with a strong emission peak observed at around 600 nm, attributed to defect states in the anatase TiO₂ nanoparticle [9]. The PL spectra display this emission peak for both samples, which is commonly linked to oxygen vacancies in the TiO₂ lattice. The Guava-derived TiO₂ sample shows a significantly higher PL intensity compared to the Neem-derived TiO₂ sample, suggesting a higher rate of radiative recombination of photo-generated electron-hole pairs [8, 10]. This elevated PL intensity in the Guava sample indicates a greater concentration of surface or bulk defects. In contrast, the

Neem sample exhibits a lower PL intensity, pointing to more effective charge carrier separation and reduced recombination—an advantage for photocatalytic applications. Although both samples emit at similar wavelengths, the variation in PL intensity reflects differences in their electronic or structural properties, which may result from differences in synthesis approaches, plant extract composition, or processing conditions.

4.7 Photocatalytic Activity

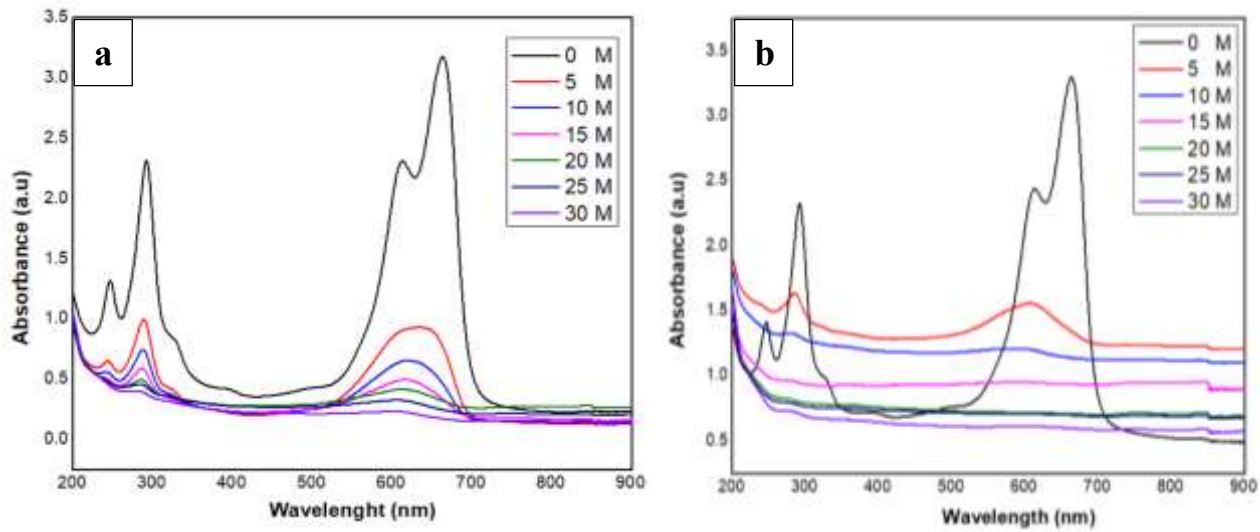


Figure. 7 UV-Vis absorption spectra of Biosynthesized TiO₂ nanoparticles + MB Solution exposure to UV light
(a) *A. indica* (Neem) & (b) *P. guajava* (Guava)

The photocatalytic activity of biosynthesized TiO₂ nanoparticles (NPs), calcinated at 600 °C and synthesized using *A. indica* (Neem) and *P. guajava* (Guava) leaf extracts, was evaluated through the degradation of methylene blue (MB) dye under ultraviolet (UV) irradiation. The time-dependent degradation profiles of MB for both TiO₂ samples are illustrated in Figure 7.

The absorption spectra revealed a gradual decrease in the intensity of the characteristic MB peak at 664 nm with increasing irradiation time for both samples, indicating the effective photodegradation of the dye molecules. The reduction in absorbance intensity demonstrates the photocatalytic activity of the biosynthesized TiO₂ nanoparticles. However, variations in degradation efficiency were observed between the two samples, likely due to differences in surface properties and electron–hole recombination rates [6], as supported by the photoluminescence (PL) spectra shown in Figure 6. Higher PL intensity corresponds to higher recombination rates, which adversely affect photocatalytic performance.

Upon increasing the irradiation time from 0 to 30 minutes, a continuous decline in absorbance intensity was noted, indicating progressive degradation of MB dye molecules. The photocatalytic degradation efficiency (X%) was calculated using the following equation [8, 18]:

$$X\% = \frac{C_0 - C}{C_0} \times 100$$

where X is the photo degradation efficiency, C₀ is the initial concentration of dye and C is the dye concentration at irradiation time t.

The degradation efficiencies of the TiO₂ NPs synthesized using Neem extract were found to be 70%, 79%, 84%, 86%, 89%, and 90% at different time intervals up to 30 minutes. In comparison, the efficiencies of the TiO₂ NPs synthesized using Guava extract were 52%, 63%, 70%, 76%, 77%, and 81%, respectively. These results indicate that the TiO₂ nanoparticles synthesized using Neem leaf extract exhibit superior photocatalytic performance compared to those synthesized using Guava leaf extract, likely due to enhanced charge carrier separation and reduced recombination rates.

4.8 Antibacterial Activity

Table 1.2 Antibacterial Activity of Biosynthesized TiO₂ NPs Against *E. coli* and *S. aureus*

Organisms Concentration (μ l)	Zone of Inhibition (mm)			
	Neem Leaf TiO ₂ NPs		Guava Leaf TiO ₂ NPs	
	<i>E.Coli</i>	<i>S. aureus</i>	<i>E.Coli</i>	<i>S. aureus</i>
25	2	1	1	2
50	3.2	2	2	3
75	3.5	3	3	4
100	4	4	5	5
Standard	10	10	10	10

The antibacterial activity of biosynthesized TiO₂ nanoparticles using Neem and Guava leaf extracts was evaluated against *Escherichia coli* (*E. coli*) and *Staphylococcus aureus* (*S. aureus*) at different concentrations (25–100 μ L) [19]. The results revealed a concentration-dependent enhancement in the zone of inhibition for both types of nanoparticles across both bacterial strains [22], as summarized in Table 1.2.

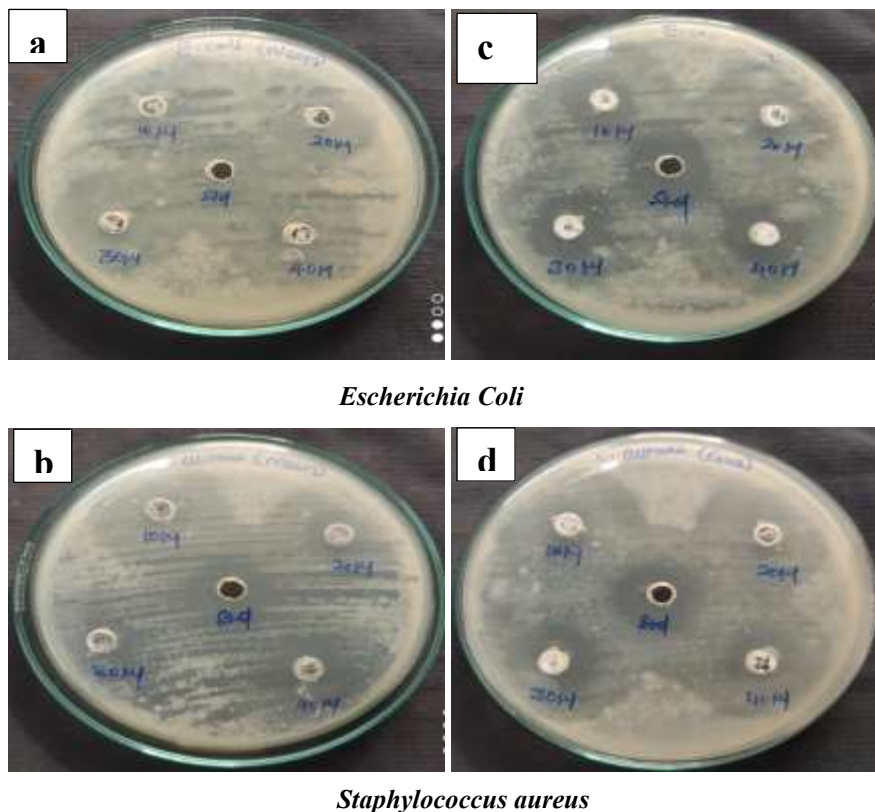


**Figure. 8 Antibacterial Activity of Biosynthesized TiO₂ nanoparticles
(a, b) *A. indica* (Neem) & (c, d) *P. guajava* (Guava)**

Figure 8 (a, b) shows the antibacterial activity against *E. coli*. The TiO₂ nanoparticles synthesized using Neem leaf extract exhibited inhibition zones of 2.0 mm, 3.2 mm, 3.5 mm, and 4.0 mm at concentrations of 25 µL, 50 µL, 75 µL, and 100 µL, respectively. In contrast, the Guava-based TiO₂ nanoparticles showed comparatively lower antibacterial activity at lower concentrations, with zones measuring 1.0 mm, 2.0 mm, 3.0 mm, and a maximum of 5.0 mm at 100 µL.

Similarly, Figure 8 (c, d) shows the antibacterial activity against *S. aureus*. The Neem-based TiO₂ nanoparticles produced inhibition zones of 1.0 mm, 2.0 mm, 3.0 mm, and 4.0 mm with increasing concentrations. The Guava-based nanoparticles demonstrated slightly higher activity at the same concentrations, with inhibition zones of 2.0 mm, 3.0 mm, 4.0 mm, and 5.0 mm at 25 µL to 100 µL, respectively.

The standard antibiotic (10 µg/disc) produced a consistent inhibition zone of 10 mm for both bacterial strains, indicating that while the biosynthesized nanoparticles exhibit notable antibacterial activity, it is moderate in comparison to commercial antibiotics. However, the results suggest that increasing the concentration of the biosynthesized TiO₂ nanoparticles enhances antibacterial efficacy. Overall, TiO₂ nanoparticles derived from Guava extract demonstrated better performance against *S. aureus*, while Neem-derived nanoparticles were slightly more effective against *E. coli* at higher concentrations.

5. Conclusion

In conclusion, this study highlights the successful biosynthesis of TiO₂ nanoparticles using aqueous leaf extracts from *Azadirachta indica* (neem) and *Psidium guajava* (guava), providing an eco-friendly alternative to conventional chemical synthesis. The nanoparticles were characterized using a range of techniques, including XRD, FTIR, FESEM, EDAX, UV-Vis, and PL, confirming their crystalline structure, elemental purity, and the involvement of phytochemicals from the leaf extracts in the synthesis process. The XRD analysis revealed the presence of anatase phase TiO₂ with characteristic peaks at 25.54°, 38.04°, and 48.25°, while FTIR spectra confirmed the formation of Ti–O bonds. The UV-Vis analysis showed absorption peaks at 313 nm for neem-derived TiO₂ and 314 nm for guava-derived TiO₂, with bandgap energies of 4.04 eV and 4.03 eV, respectively. The photodegradation of methylene blue showed that neem-derived TiO₂ achieved degradation efficiencies of 90% after 30 minutes of UV irradiation, while guava-derived TiO₂ reached 81%. The antibacterial activity revealed concentration-dependent inhibition, with Neem-derived nanoparticles showing inhibition zones of 4.0 mm against *E. coli* at 100 µL, while Guava-derived nanoparticles exhibited maximum inhibition zones of 5.0 mm against *S. aureus*. These results underscore the potential of green-synthesized TiO₂ nanoparticles for photocatalytic and antimicrobial applications, offering a sustainable and effective approach to nanomaterial synthesis.

Reference:

1. M. Singh, et al., Green synthesis of Neem-based Zinc Oxide and Titanium Dioxide nanoparticles for enhanced antimicrobial functionalization of DBD plasma treated silk and corn fabrics, *NanoWorld J.*, 9(Suppl. 5), (2023).
2. B.K. Thakur, et al., Green synthesis of titanium dioxide nanoparticles using *Azadirachta indica* leaf extract and evaluation of their antibacterial activity, *S. Afr. J. Bot.*, 124, 223–227 (2019).

3. S. Sagadevan, et al., A comprehensive review on green synthesis of titanium dioxide nanoparticles and their diverse biomedical applications, *Green Process. Synth.*, 11, 44–63 (2022).
4. M. Saeed, et al., *Azadirachta indica* leaves extract assisted green synthesis of Ag–TiO₂ for degradation of Methylene Blue and Rhodamine B dyes in aqueous medium, *Green Process. Synth.*, 8, 659–666 (2019).
5. T. Santhoshkumar, et al., Green synthesis of titanium dioxide nanoparticles using *Psidium guajava* extract and its antibacterial and antioxidant properties, *Asian Pac. J. Trop. Med.*, 7(12), 968–976 (2014).
6. M. Ganeshbabu, et al., Synthesis and characterization of BiVO₄ nanoparticles for environmental applications, *RSC Adv.*, 10, 18315–18322 (2020).
7. P. Thammaacheep, et al., Bio-synthesis of TiO₂ photocatalyst: a reduced step approach using leaf extract, *Green Chem. Lett. Rev.*, 17(1), 2433607 (2024).
8. N. Nithya, et al., Neodymium doped TiO₂ nanoparticles by sol-gel method for antibacterial and photocatalytic activity, *Mater. Sci. Semicond. Process.*, 83, 70–82 (2018).
9. C. Jin, et al., Structure and photoluminescence of the TiO₂ films grown by atomic layer deposition using tetrakis-dimethylamino titanium and ozone, *Nanoscale Res. Lett.*, 10, 95 (2015).
10. S.A. Abdullah, et al., Photoluminescence study of trap-state defect on TiO₂ thin films at different substrate temperature via RF magnetron sputtering, *IOP Conf. Ser.: J. Phys.: Conf. Ser.*, 995, 012067 (2018).
11. S.A. Hamdan, et al., Comparison of anatase and rutile TiO₂ nanostructures for gas sensing application, *Dig. J. Nanomater. Biostruct.*, 15(4), 1001–1008 (2020).
12. S. Shekhar, et al., Green chemistry-based benign approach for the synthesis of titanium oxide nanoparticles using extracts of *Azadirachta indica*, *Clean. Eng. Technol.*, 13, 100607 (2023).
13. V. Kulkarni, et al., Bio-synthesis and characterization of titanium dioxide nanoparticles (TiO₂) using *Azadirachta indica* leaf (Neem leaf) extract, *Int. J. Curr. Microbiol. App. Sci.*, 8(10), 2309–2317 (2019).
14. H.K. Abd El-Hamid, A.A. Gaber, R.E.A. Ngida, H.E.H. Sadek, R.M. Khattab, H.S. Mandour, Study of microstructure and corrosion behavior of nano-Al₂O₃ coating layers on TiO₂ substrate via polymeric method and microwave combustion, *Sci. Rep.*, 14, 18417 (2024).
15. N.K. Sethy, Z. Arif, P.K. Mishra, P.K. Kumar, Green synthesis of TiO₂ nanoparticles from *Syzygium cumini* extract for photocatalytic removal of lead (Pb) in explosive industrial wastewater, *Green Process. Synth.*, 9, 171–181 (2020).
16. F.S. Ansari, S. Daneshjou, Optimizing the green synthesis of antibacterial TiO₂ - anatase phase nanoparticles derived from spinach leaf extract, *Sci. Rep.*, 14, 22440 (2024).
17. S. Dhiman, A. Kumari, S. Kumari, R. Sharma, Advanced biodegradable starch-based nanocomposite films incorporating zinc oxide nanoparticles: Synthesis, characterization, and efficacy in antibacterial food packaging applications, *J. Environ. Chem. Eng.*, 13(3), 116296 (2025).
18. R. Gobi, R.S. Babu, In-vitro investigation of chitosan/polyvinyl alcohol/TiO₂ composite membranes for wound regeneration, *Biochem. Biophys. Res. Commun.*, 742, 151129 (2025).
19. S.S. Salem, A. Fouda, Green synthesis of metallic nanoparticles and their prospective biotechnological applications: An overview, *Biol. Trace Elem. Res.*, 199, 344–370 (2021).
20. D. Ravichandran, M.A. Megala, K. Anbalagan, P. Srivastava, M.A. Al-Dosary, A.A. Hatamleh, S. Murugesan, Eco-friendly synthesis of biochar–CoFe₂O₄ nanocomposites using *Ulva lactuca* L. for

- photocatalytic degradation of Congo red and in vitro biological applications, *Colloids Surf. A Physicochem. Eng. Asp.*, 713, 136465 (2025).
21. K. Manimaran, D.H.Y. Yanto, F.C. Ardiati, M. Oktaviani, D. Natarajan, C. Ragavendran, C. Kamaraj, B. Karunanithi, S. Loganathan, Enhanced photocatalytic degradation, antimicrobial and anticancer efficiency of mycosynthesized TiO₂ nanoparticles using *Pleurotus ostreatus* mushroom extract: An eco-friendly approach, *J. Environ. Chem. Eng.*, 11(6), 111512 (2023).
22. M. Taran, M. Rad, M. Alavi, Biosynthesis of TiO₂ and ZnO nanoparticles by *Halomonas elongata* IBRC-M 10214 in different conditions of medium, *Bioimpacts*, 8(2), 81–89 (2018).